Robust direct effect of carbon dioxide on tropical circulation and regional precipitation

Author:

Bony, S; Pellon, G; Klocke, D; Sherwood, Steven; Fermepin, S; Denvil, S

Robust direct effect of carbon dioxide on tropical circulation and regional precipitation

Sandrine Bony[1,*], Gilles Bellon[2], Daniel Klocke[3], Steven Sherwood[4], Solange Fermepin[1] and Sébastien Denvil[1]

[1]*LMD/IPSL, CNRS, Université Pierre et Marie Curie, Paris, France*

[2]*CNRM/GAME, CNRS, Météo-France, Toulouse, France*

[3]*European Centre for Medium-Range Weather Forecasts, Reading, United Kingdom*

[4]*CCRC and Centre of Excellence for Climate System Science, Univ. New South Wales, Sydney, Australia*

Predicting the response of tropical rainfall to climate change remains a scientific challenge[1]. Rising atmospheric concentrations of carbon dioxide are expected to affect the hydrological cycle through global temperature and water vapour increases[2–4]. However, regional precipitation changes also closely depend on the atmospheric circulation, which is expected to weaken in a warmer atmosphere[4–6]. Here, physically-based analyses of simulations from multiple state-of-the-art climate models in a large spectrum of configurations and from an operational Numerical Weather Prediction model show that about half the tropical circulation changes projected by the end of the century in a scenario with no mitigation, and thus a large part of regional precipitation changes, is independent of global surface warming. It results instead from the effect of increased carbon dioxide on the radiative cooling of the atmosphere, having an immediate impact on the strength of atmospheric vertical mo-

tions. These robust results imply that preventing future rainfall changes in the tropics would require preventing not only global warming, as envisioned in some geo-engineering proposals, but also avoiding further increases in the amount of carbon dioxide in the atmosphere. Strategies that may help constrain rainfall projections using climate and weather observations are suggested.

Human activities have raised the carbon dioxide (CO_2) concentration in the atmosphere, and further rise seems inevitable during the next decades. Difficulties in quantifying climate feedbacks[7] make the estimate of the global warming associated with increased CO_2 uncertain, and the estimate of regional precipitation changes induced by surface warming even more uncertain. These are of particular concern in the tropics where human welfare closely depends on rainfall. However, several studies have shown that CO_2 could also impact the atmosphere through fast adjustments independent of surface temperature changes[2,8]. How much, then, do regional precipitation changes projected by the end of the century depend on the surface warming?

We address this question by analysing a suite of numerical simulations from 16 state-of-the-art coupled ocean-atmosphere general circulation models (OAGCMs) participating in the Fifth Phase of the Coupled Models Inter-comparison Project (CMIP5[9], see Methods and Supplementary Material). Assuming a socio-economic pathway where humans continue to use fossil fuels with no mitigation ("RCP8.5" scenario[10]), these models project by the end of the 21st century a tropical (30°S-30°N) mean surface warming relative to pre-industrial temperatures of 4.2 K (with a standard deviation of 1.1 K), larger over land than over ocean, and large changes in the regional distribution

of rainfall (ΔP, Figure 1).

We interpret the response of tropical precipitation by dividing it into two components[4, 11–14]: a dynamic one due to circulation changes, and one independent of these (see Methods). Using the vertically-averaged large-scale vertical (pressure) air velocity $\bar{\omega}$ (defined positive for downward motions) as a proxy for large-scale atmospheric motions, we diagnose the dynamic component (ΔP_{dyn}) as the contribution to ΔP from changes in $\bar{\omega}$. The remaining change is referred to as the thermodynamic component, ΔP_{ther}, i.e., $\Delta P = \Delta P_{\text{dyn}} + \Delta P_{\text{ther}}$.

The multi-model mean ΔP_{ther} exhibits a "wet get wetter, dry get drier" regional pattern[4] (Figure 1). This is primarily explained by the increase of atmospheric water vapour with temperature (following the Clausius-Clapeyron relationship), and the associated increase of moisture convergence in the moist, rising branches of the present-day tropical circulation and moisture divergence from the dry, subsidence regions (Supplemental Figure S2). This pattern, which is also found in observed trends[15, 16], is thus closely related to the climatological distribution of precipitation. In contrast, circulation changes lead to a more complex pattern of precipitation changes (ΔP_{dyn}), which explains a large part of the spread of regional precipitation projections amongst climate models (about 70 % of the tropical-mean variance, Supplemental Figure S8).

The radiative forcing achieved around 2090 in the RCP8.5 scenario is equivalent to that produced by a quadrupling of the pre-industrial CO_2 concentration (4xCO_2). To assess the relative influence of increased CO_2 vs. surface warming on tropical precipitation changes, we analyse alter-

native experiments with the same models in which the atmospheric CO_2 concentration is abruptly quadrupled and then held fixed, instead of increasing progressively (See Methods). When warming in these alternate experiments reaches 4 K, simulated regional changes in rainfall are nearly identical to those forecast for 2090. This alternate scenario, however, enables us to isolate the roles of CO_2 and surface warming in producing these consistent patterns.

The multi-model mean evolution of ΔP_{ther} and ΔP_{dyn} as a function of surface warming (Figure 2) shows that the "wet get wetter, dry get drier" pattern (ΔP_{ther}) is weak shortly after the CO_2 increase, when surface warming is still small (≤ 1 K), and that it subsequently strengthens with further warming. In contrast, ΔP_{dyn} exhibits a fast response to increased CO_2 associated with large regional anomalies: precipitation increases over most land regions (partly driven by the mass convergence induced by their fast surface warming relative to the oceans), over the equatorial eastern Pacific and over subtropical dry regions, while it mostly decreases in regions of high present-day precipitation. Over land, ΔP_{dyn} weakens with surface warming in wet areas, and even changes sign in some regions (e.g., central Africa and South America). Over ocean, on the contrary, ΔP_{dyn} evolves much less with surface warming, and the fast response pattern exhibits many similarities with the long-term pattern of ΔP_{dyn}. It also forces an El-Niño-like precipitation pattern.

To interpret the behaviour of ΔP_{dyn}, we analyse the response of large-scale atmospheric vertical motions to increased CO_2 and surface warming. For this purpose, we compute the monthly average upward ($\bar{\omega}^{\uparrow}$, negative) and downward ($\bar{\omega}^{\downarrow}$, positive) pressure vertical velocities for tropical land, ocean and land+ocean areas, as well as their difference $I = \bar{\omega}^{\downarrow} - \bar{\omega}^{\uparrow}$, which may be considered

as a measure of the strength of the tropical overturning (or Hadley-Walker) circulation. In the pre-industrial climate, $\bar{\omega}^{\uparrow}$, $\bar{\omega}^{\downarrow}$ and I_c are stable in time despite small (< 2 %) interannual fluctuations.

As climate warms, OAGCMs predict a progressive weakening of $\bar{\omega}^{\uparrow}$, $\bar{\omega}^{\downarrow}$ and I_c over both land and ocean (Figure 3). This is consistent with theories and numerical studies suggesting that the tropical circulation weakens under global warming owing to the increase of the lower-tropospheric water vapour and dry static stability of the atmosphere[4–6]. However, Figure 3 also highlights a direct effect of increased CO_2 on the circulation: when surface warming is weak, the change in CO_2 induces a weakening of $\bar{\omega}^{\downarrow}$ over both land and ocean, a weakening of $\bar{\omega}^{\uparrow}$ over ocean, and a strengthening of $\bar{\omega}^{\uparrow}$ over land. This response occurs in every AOGCM examined, though with variable magnitude (Supplemental Table S2).

To confirm that these year-one changes are due mainly to CO_2 rather than the small amount of warming (≤ 1 K), and that they are robust, we examine further simulations where sea-surface temperatures (SSTs) are held fixed during the CO_2 quadrupling, both in standard models and in versions with land removed ("aqua-planets"). With standard models, the responses of $\bar{\omega}^{\downarrow}$, $\bar{\omega}^{\uparrow}$ and I_c to increased CO_2 are consistent with those predicted by OAGCMs during the first year (Figure 3), while the aqua-planet responses account for a large fraction of those predicted with continents (more than 50% of rising motions changes, nearly 100% of subsidence changes, and 70 % of changes in circulation strength). The increased CO_2 thus exerts a direct effect on large-scale vertical motions which is not primarily mediated by surface temperature changes, nor by land-sea contrasts, although the latter amplify circulation changes.

This effect on the circulation explains much of the regional pattern of ΔP_{dyn} immediately after the abrupt CO_2 quadrupling (Figure 2): over most land regions, precipitation increases owing to the strengthening of $\bar{\omega}^{\uparrow}$ and the weakening of $\bar{\omega}^{\downarrow}$; over ocean precipitation increases in regions of present-day subsidence, and decreases in regions of present-day convection and high rain, consistently with the weakening of $\bar{\omega}^{\downarrow}$ and $\bar{\omega}^{\uparrow}$, respectively. Over ocean, comparing the impact on $\bar{\omega}^{\uparrow}$ of CO_2-only versus that of CO_2 plus global warming (Figure 3) shows that the direct effect of CO_2 explains about half of the weakening of large-scale ascent in the tropics simulated by climate models by the end of the century. Systematic changes of precipitation averaged over present-day wet and dry regions from direct CO_2 forcing are of comparable magnitude to those from warming (Supplemental Figure S1).

How does CO_2 change the circulation? By reducing the loss of infrared radiation to space more than it affects the radiation at the surface, higher CO_2 concentrations weaken the net radiative cooling of the atmosphere. CO_2 thus exerts its direct effect by warming and slightly stabilising the atmosphere, and by warming the continents relative to the oceans due to the former's low heat capacity. Regional circulation responses on land are certainly sensitive to both[17,18]. However, the response of the overall overturning circulation is similar in models with and without continents (Figure 3), indicating that it is driven mainly by the atmospheric heating.

To test this explanation, we run a single-column model (SCM) in the weak temperature gradient approximation[19], i.e. in a configuration where the large-scale vertical velocity can be predicted for a range of sea surface temperature values, given free-tropospheric temperatures which at low

6

latitudes are fairly uniform (see Methods). The model qualitatively reproduces the subsidence over cooler SSTs and ascent over warmer SSTs seen in GCMs (Figure 4). Moreover, when this model is rerun with 4xCO$_2$ and the slightly warmer (hence more stable) mean temperature profile simulated by the GCMs under this condition, it also reproduces the weakening of both descent and ascent (Figure 4). Surface warming and land-sea contrasts are thus not the primary drivers of changes in the overturning circulation.

On what time scale does this dynamic adjustment occur? A climate model used in a "Numerical Weather Prediction" (NWP) mode[20] (see Methods) but forced by an abrupt CO$_2$ quadrupling, shows that the circulation begins to change on the very first day, and that about half the 30-year mean change from 4xCO$_2$ is achieved within only five days (Figure 4). The CO$_2$ direct effect on circulation thus relies on fast physical processes. This calls for examining it in a GCM carefully evaluated on short time scales. For this purpose, we use the European Centre for Medium Range Weather Forecasts (ECMWF) Integrated Forecast System (IFS) operational model[21] and perform 10-day forecasts of the atmosphere for two months (October and April 2011) for 1xCO$_2$ or 4xCO$_2$ concentrations (see Methods). This model also predicts a fast circulation response over ocean (Figure 4), and an enhancement of upward motions and precipitation over land (Supplemental Figure S7). Over ocean, the weakening of upward motions occurs faster than that of subsidence. In convective areas associated with large-scale upward motions, the magnitude of the response after 10 days is comparable to that predicted on average over 30 years by CMIP5 atmospheric models.

The fast and direct effect of CO$_2$ on tropical vertical motions is thus physically understood

7

and predicted by multiple climate models in a large spectrum of configurations and complexities. It is also predicted by a model that explicitly simulates individual cloud systems[22]. This robust result implies that part of the tropical precipitation response to climate change is independent of how much the surface warms. It also explains, for example, findings that "geo-engineering" options aiming at weakening global warming without removing CO_2 from the atmosphere would fail to fully mitigate precipitation changes at global or regional scales[23,24].

We conclude that regional precipitation responses to climate change are driven largely by physical mechanisms which are robust across climate models (Supplementary Material). So why do regional precipitation projections differ so much among models? Our study suggests at least three reasons. First, the correlation between ΔP_{ther} and the precipitation climatology implies that model differences in the simulation of the present-day climate translate into different patterns of precipitation change (Supplemental Figures S3 and S4). Fortunately, observations of the former should help reduce uncertainty in the latter. Second, models still exhibit a large range of climate sensitivity estimates[25]. This alters the magnitude of ΔP_{ther} relative to ΔP_{dyn} and the sign of ΔP_{dyn} over land, which adds uncertainty in the overall response (Figure 2). Reducing the uncertainty in climate sensitivity will thus translate into a significant reduction of the precipitation projection uncertainty. Third, ΔP_{dyn} is only partly constrained by the physical arguments explored here and exhibits significant variations between models, partly due to the CO_2-driven response (Supplementary Material). The latter being controlled by fast physical processes, however, supports the strategy of understanding it through process evaluations and weather-forecast simulations on very short time scales[20]. Such studies could also help constrain climate sensitivity

estimates[8, 25, 26]. Therefore long-standing uncertainties in climate projections may be decomposed into more tractable components, that may be more easily understood and constrained individually using climate and weather observations. Ultimately, this should help increase confidence in future climate change assessments.

Methods

Atmospheric circulation diagnostics in CMIP5 models. Monthly-mean CMIP5 climate model outputs were retrieved from the Earth System Grid Federation archive ($http : //cmip-pcmdi.llnl.gov/cmip5$). The list of CMIP5 models considered in this study is given in Supplementary Material. We use single realisations of several CMIP5 experiments[9]: 30-year time slices of pre-industrial and abrupt $4xCO_2$ coupled ocean-atmosphere experiments, 30-year atmosphere-only simulations forced by a fixed $1xCO_2$ or $4xCO_2$ concentration and using a prescribed SST distribution, 5-year aqua-planet experiments and 20-year time slices (2080-2099) of RCP8.5 experiments. For each CMIP5 simulation and model, we compute the vertical average $\bar{\omega}$ of pressure vertical velocity profiles, the Probability Distribution Function $P_{\bar{\omega}}$ of $\bar{\omega}$ in the tropics[7] and the tropical-mean upward and downward vertical velocities over land, ocean and land+ocean regions.

Dynamic and thermodynamic components of precipitation changes. The monthly-mean vertically-integrated water budget is diagnosed at the regional scale for each model and each numerical experiment using (e.g. [27]) : $P = E - \left[q\vec{\nabla}.\vec{V} \right] - \left[\vec{V}.\vec{\nabla}q \right]$, where P is the precipitation, E the surface evaporation, $\vec{V}$ the horizontal wind, and q the vertical profile of specific humidity. Brackets refer to mass-weighted vertical integrals. We note H_q the vertically-integrated hor-

9

izontal moisture advection term $(-\left[\vec{V}.\vec{\nabla}q\right])$. Using mass continuity and after integration by parts over the depth of the troposphere, the term $-\left[q\vec{\nabla}.\vec{V}\right]$ is equal to $-\left[\omega\partial q/\partial\tilde{P}\right]$, where ω is the vertical profile of pressure vertical velocity and $\tilde{P}$ the atmospheric pressure. As in the tropics the vertical structure of ω is close to a first baroclinic mode, we decompose ω as $\omega = \Omega + (\omega - \Omega)$, where Ω is a vertical velocity profile of vertically-averaged value $\bar{\omega}$ and defined by $\Omega(\tilde{P}) = \bar{\omega}\Phi(\tilde{P})$. Φ is a specified vertical structure (a cubic polynomial vanishing at 1013 hPa and 100 hPa and having a maximum at 600 hPa, such that $\int_{100}^{1013} \Phi(\tilde{P})\,d\tilde{P}/g = 1$ where g is the gravitational acceleration). Then $P = E + \bar{\omega}\Gamma_q + V_q^\alpha + H_q$, with $\Gamma_q = -\left[\Phi(\tilde{P})\frac{\partial q}{\partial \tilde{P}}\right]$ and $V_q^\alpha = -\left[(\omega(\tilde{P}) - \Omega(\tilde{P}))\frac{\partial q}{\partial \tilde{P}}\right]$. The change in monthly-mean precipitation can then be expressed as : $\Delta P = (\Delta E + \bar{\omega}\Delta\Gamma_q + \Delta H_q + \Delta V_q^\alpha) + \Gamma_q\Delta\bar{\omega} = \Delta P_{ther} + \Delta P_{dyn}$, with $\Delta P_{dyn} = \Gamma_q\Delta\bar{\omega}$. The term ΔP_{dyn} is referred to as the dynamic component because it is directly related to the change in $\bar{\omega}$. The other component, ΔP_{ther}, is referred to as the thermodynamic component because it is largely dominated by the Clausius-Clapeyron relationship (see Supplementary Material).

Single Column Model simulations. SCM simulations of the tropical atmosphere in $1xCO_2$ and $4xCO_2$ conditions are performed with the IPSL-CM5A-LR atmospheric GCM[28,29]. In the Weak Temperature Gradient approximation, justified by the weakness of horizontal temperature gradients in the tropical free troposphere, ω and its associated moisture convergence can be diagnosed from energy balance, given the temperature profile[19]. In our setup, the temperature profile of the SCM in the free troposphere (i.e., at pressures lower than 800 hPa) is relaxed towards a specified tropical-mean temperature profile[30] derived from an atmospheric GCM (IPSL-CM5A-LR) simulation (in $1xCO_2$ or $4xCO_2$ conditions). Within the boundary layer, the vertical velocity is assumed to vary

linearly with pressure and to vanish at the surface. Simulations are performed for $1xCO_2$ and $4xCO_2$ concentrations, for varying SSTs and fixed surface wind (7 m/s, close to the tropical-mean value).

Numerical Weather Prediction simulations. Short-term simulations of the global atmosphere are performed for two values of the CO_2 concentration ($1xCO_2$ or $4xCO_2$) with two models : the atmospheric component[28] of the CMIP5 IPSL-CM5A-LR OAGCM[29] initialised with the ECMWF Year of Tropical Convection (YOTC, $http://data-portal.ecmwf.int/data/d/yotc\_od/$) analysis dataset for each day of January, April, July and October 2009 at 00UTC, and the current version (CY37r2) of the ECMWF-IFS model initialised with its own corresponding analysis (at 00, 06, 12 and 18 UTC) for the months of April and October 2011. The ability of the ECMWF-IFS model to simulate fast physical processes is routinely assessed with two weather forecasts per day over several years[21]. For each month (in $1xCO_2$ or $4xCO_2$), we average the model outputs at fixed forecast times (1 day, 5 days etc), and we stratify the regional monthly-mean $\bar{\omega}$ by the monthly SST using 1 K bins.

1. Solomon, S. et al. Technical Summary. In: *Climate Change 2007: The Physical Science Basis. Contribution of Working Group I to the Fourth Assessment Report of the Intergovernmental Panel on Climate Change*, edited by S. Solomon, D. Qin, M. Manning, Z. Chen, M. Marquis, K.B. Averyt, M. Tignor and H.L. Miller, Cambridge University Press, Cambridge, United Kingdom and New York, NY, USA (2007).

2. Mitchell, J. F. B. The seasonal response of a general circulation model to changes in CO_2 and

sea temperatures. *Quart. J. Roy. Meteor. Soc.* **109**, 113-152 (1983)

3. Allen, M. R. & Ingram, W. J. Constraints on future changes in the hydrological cycle. *Nature* **419**, 224-228 (2002).

4. Held, I. M. & Soden, B. J. Robust responses of the hydrological cycle to global warming. *J. Clim.* **19**, 5686-5699 (2006)

5. Knutson, T. R. & Manabe, S. Time-mean response over the tropical Pacific to increased CO_2 in a coupled ocean-atmosphere model. *J. Clim.* **8**, 2181-2199 (1995).

6. Vecchi, G. A. & Soden, B. J. Global warming and the weakening of the tropical circulation. *J. Clim.* **20** 4316-4340 (2007).

7. Bony S. et al. How well do we understand and evaluate climate change feedback processes? *J. Clim.* **19**, 3445-3482 (2006).

8. Gregory, J. M. & Webb, M. J. Tropospheric adjustment induces a cloud component in CO_2 forcing. *J. Clim.* **21**, 58-71 (2008)

9. Taylor, K. E., Stouffer, R. J. & Meehl, G. A. An Overview of CMIP5 and the experiment design. *Bull. Amer. Meteor. Soc.*, **93**, 485-498, doi:10.1175/BAMS-D-11-00094.1 (2012).

10. Moss, R. et al. A new approach to scenario development for the IPCC Fifth Assessment Report. *Nature*, **463**, doi:10.1038/nature08823 (2010).

11. Emori, S. & Brown, S. J. Dynamic and thermodynamic changes in mean and extreme precipitation under changed climate. *Geophys. Res. Lett.* **32**, L17706 (2005).

12. Chou, C., Neelin, J. D., Chen, C.-A. & Tu, J.-Y. Evaluating the "Rich-Get-Richer" Mechanism in Tropical Precipitation Change under Global Warming. *J. Clim.* **22**, 1982-2005 (2009).

13. Seager, R., Naik, N. & Vecchi, G. A. Thermodynamic and dynamic mechanisms for large-scale changes in the hydrological cycle in response to global warming. *J. Clim.* **23**, 4651-4668 (2010).

14. Muller, C. J. & O'Gorman, P. A. An energetic perspective on the regional response of precipitation to climate change. *Nature Clim. Change* **1**, 266-271 (2011).

15. Liu, C., Allan, R. P. & Huffman, G. J., Co-variation of temperature and precipitation in CMIP5 models and satellite observations. *Geophys. Res. Lett.* **39**, L13803, doi:10.1029/2012GL052093 (2012).

16. Chou, C., Chiang, J. C. H., Lan, C.-W., Chung, C.-H., Liao, Y.-C. & Lee, C.-J., Increase in the range between wet and dry season precipitation. *Nature Geosci.*, doi:10.1038/ngeo1744 (2013).

17. Joshi, M., Gregory, J., Webb, M., Sexton, D. & Johns, T. Mechanisms for the land-sea warming contrast exhibited by simulations of climate change. *Clim. Dyn.* **30**, 455-465 (2008).

18. Cao, L., Bala, G. & Caldeira, K. Climate response to changes in atmospheric carbon dioxide and solar irradiance on the time scale of days to weeks. *Environ. Res. Lett.* **7**, doi:10.1088/1748-9326/7/3/034015 (2012).

19. Sobel, A. H. & Bretherton, C. S. Modeling tropical precipitation in a single column. *J. Clim.* **13**, 4378-4392 (2000)

20. Phillips, T.J. et al. Evaluating parameterizations in general circulation models: Climate simulation meets weather prediction. *Bull. Am. Meteorol. Soc.* **85**, 1903-1915 (2004).

21. Bechtold, P. et al. Advances in simulating atmospheric variability with the ECMWF model: From synoptic to decadal time-scales. *Q. J. R Meteorol. Soc.* **134**, 1337-1351 (2008).

22. Wyant, M. C., Bretherton, C. S., Blossey, P. N. & Khairoutdinov, M. Fast cloud adjustment to increasing CO_2 in a superparameterized climate model. *JAMES* **4**, M05001 (2012).

23. Bala, G., Duffy, P. B. & Taylor, K. E. Impact of geoengineering schemes on the global hydrological cycle. *P. Natl. Acad. Sci. USA*. **105**, 7664-7669, doi:10.1073/pnas.0711648105 (2008).

24. Schmidt, H. et al. Solar irradiance reduction to counteract radiative forcing from a quadrupling of CO_2: climate responses simulated by four Earth System Models. *Earth Syst. Dynam.* **3**, 6378 (2012).

25. Andrews, T., Gregory, J., Webb, M. & Taylor, K. Forcing, feedbacks and climate sensitivity in CMIP5 coupled atmosphere-ocean climate models. *Geophys. Res. Lett.*, **39**(9), L09,712 (2012)

26. Rodwell, M. & Palmer, T. N. Using numerical weather prediction to assess climate models. *Q. J. R Meteorol. Soc*. **133**, 129-146 (2009).

27. Neelin, J. D. Moist dynamics of tropical convection zones in monsoons, teleconnections and global warming. In *The Global Circulation of the Atmosphere*, T. Schneider and A. Sobel, Eds, Princeton University Press, Princeton, 385pp. (2007).

28. Hourdin, F. et al. The LMDZ general circulation model: Climate performance and sensitivity to parameterized physics with emphasis on tropical convection. *Clim. Dyn.* **19**, 3445-3482 (2006)

29. Dufresne, J.-L. et al. Climate change projections using the IPSL-CM5 Earth System Model: from CMIP3 to CMIP5, *Clim. Dyn.*, DOI: 10.1007/s00382-012-1636-1, in press.

30. Raymond, D. J. & Zeng, X. Modelling tropical atmospheric convection in the context of the weak temperature gradient approximation. *Quart. J. Roy. Meteor. Soc.*, **131**, 1301-1320 (2005).

Author contributions S.B. designed the study and performed the analysis. G.B. designed and performed single-column simulations, S.F. designed and performed short-term IPSL simulations, D.K. designed and performed ECMWF forecasts and contributed to the graphics. S.D. organised the retrieval of CMIP5 model

outputs. S.B. and S.S. wrote the paper. All authors discussed the results and edited the manuscript.

Figure 1 Multi-model mean projection of tropical precipitation changes at the end of the **21st century. a**, Climatological multi-model mean annual precipitation simulated by sixteen CMIP5 climate models in the pre-industrial climate. **b**, Multi-model mean change in annual precipitation projected by the same models and its decomposition ($\Delta P = \Delta P_{\text{ther}} + \Delta P_{\text{dyn}}$) into thermodynamic (**c**, ΔP_{ther}) and dynamic (**d**, P_{dyn}) components at the end of the 21st century in a climate change scenario without mitigation (RCP8.5).

Figure 2 Interpretation of the multi-model mean regional pattern of tropical precipitation **changes induced by a CO_2 increase.** Decomposition into thermodynamic (**a-d**, ΔP_{ther}) and dynamic (**e-h**, ΔP_{dyn}) components of the annual-mean precipitation change predicted by CMIP5 coupled ocean-atmosphere models at different stages of an experiment in which CO_2 is abruptly quadrupled: (**a, e**) for the first year after CO_2 quadrupling, and for a tropical surface warming of (**b, f**) 2 K, (**c, g**) 3 K, (**d, h**) 4 K. Note the resemblance between the patterns simulated for a 4 K surface warming in this experiment and those projected by the end of the 21st century in the RCP 8.5 scenario (Figure 1c-d).

Figure 3 Response of the tropical atmospheric circulation to increased CO_2 in a range **of CMIP5 experiments.** For land (in red) and ocean (in blue) areas, evolution with surface warming of the multi-model mean fractional change (compared to pre-industrial) in tropical-mean upward ($\bar{\omega}^{\uparrow}$, **a**) and downward ($\bar{\omega}^{\downarrow}$, **b**) vertical velocities, and in the strength of the overturning circulation (I, **c**) predicted by coupled ocean-atmosphere models after an abrupt CO_2 quadrupling (solid circles, shown only when at least 10 model results are

available). Also reported are estimates from the non-mitigated RCP8.5 climate change scenario around 2090 (open squares), and from $4xCO_2$ atmosphere-only experiments with fixed SSTs in realistic (stars) and aqua-planet (open circles) configurations. Vertical bars show $\pm$ one standard deviation of individual model results around the multi-model mean.

Figure 4 **Interpretation and time scale of the direct effect of CO_2 on large-scale vertical motions.** Monthly-mean $\bar{\omega}$ predicted by CMIP5 atmospheric GCMs over tropical oceans composited by sea-surface temperatures (SSTs) in the present-day climate (**a**), and its change when atmospheric CO_2 is quadruped but SSTs are kept unchanged ($4xCO_2$-$1xCO_2$, **b**). The black line shows multi-model mean values and the shaded area the inter-model standard deviation within each SST bin. Results from single-column (1D) simulations run in the "weak temperature gradient" approximation are shown by green stars. These simulations are compared with short atmospheric forecasts (at fixed forecast times) performed in $1xCO_2$ and $4xCO_2$ conditions using either a climate model (IPSL-CM5A) or an operational weather forecasting model (ECMWF).
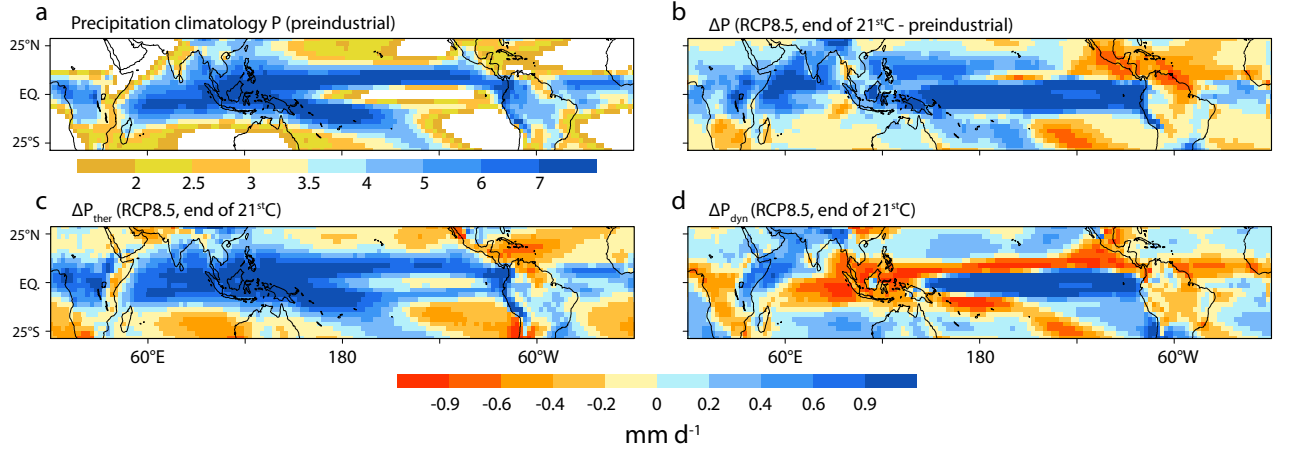
Figure 1: **Multi-model mean projection of tropical precipitation changes at the end of the 21st century. a**, Climatological multi-model mean annual precipitation simulated by sixteen CMIP5 climate models in the pre-industrial climate. **b**, Multi-model mean change in annual precipitation projected by the same models and its decomposition ($\Delta P = \Delta P_{\text{ther}} + \Delta P_{\text{dyn}}$) into thermodynamic (**c**, ΔP_{ther}) and dynamic (**d**, P_{dyn}) components at the end of the 21st century in a climate change scenario without mitigation (RCP8.5).
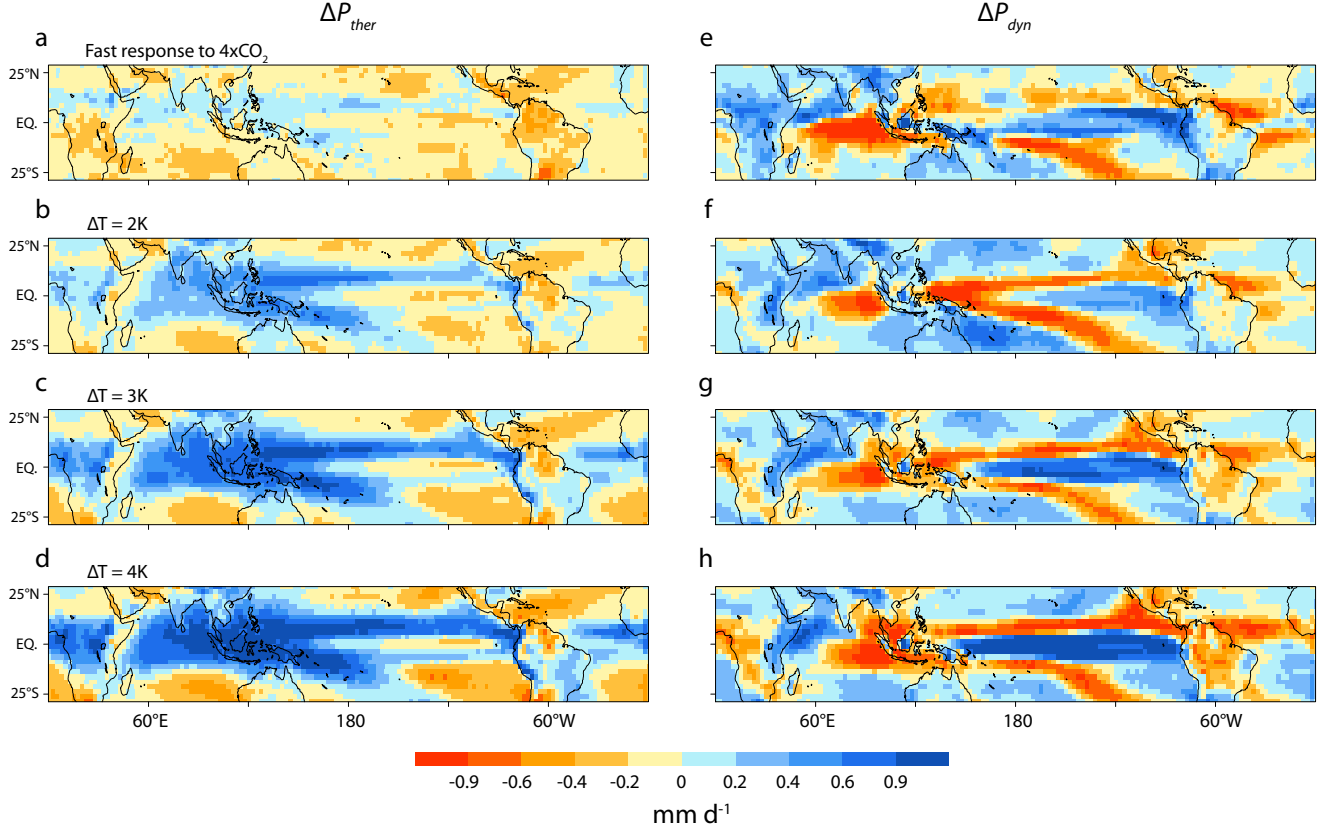
1

Figure 2: **Interpretation of the multi-model mean regional pattern of tropical precipitation changes induced by a CO_2 increase.** Decomposition into thermodynamic (**a-d**, ΔP_{ther}) and dynamic (**e-h**, ΔP_{dyn}) components of the annual-mean precipitation change predicted by CMIP5 coupled ocean-atmosphere models at different stages of an experiment in which CO_2 is abruptly quadrupled: (**a, e**) for the first year after CO_2 quadrupling, and for a tropical surface warming of (**b, f**) 2 K, (**c, g**) 3 K, (**d, h**) 4 K. Note the resemblance between the patterns simulated for a 4 K surface warming in this experiment and those projected by the end of the 21$^{\text{st}}$ century in the RCP 8.5 scenario (Figure 1c-d).
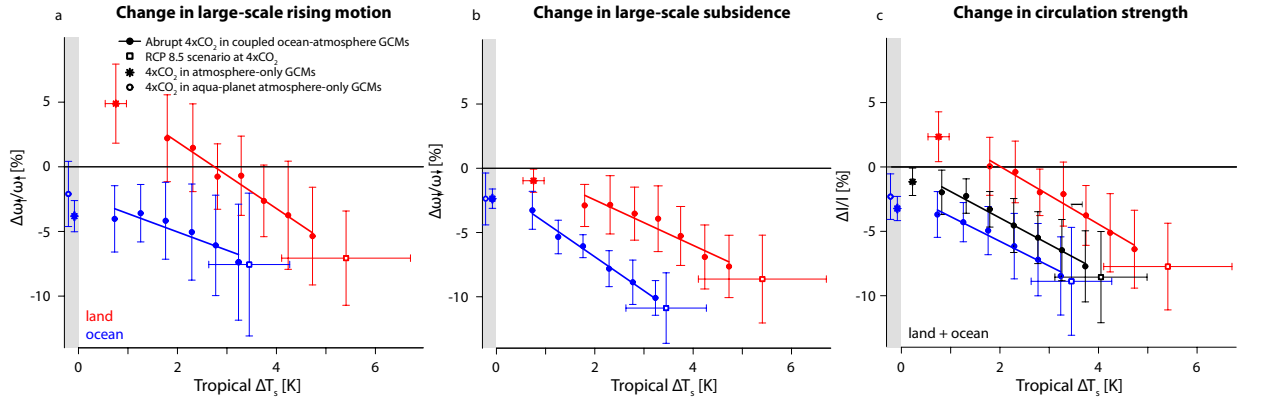
Figure 3: **Response of the tropical atmospheric circulation to increased CO_2 in a range of CMIP5 experiments.** For land (in red) and ocean (in blue) areas, evolution with surface warming of the multi-model mean fractional change (compared to pre-industrial) in tropical-mean upward ($\bar{\omega}^{\uparrow}$, **a**) and downward ($\bar{\omega}^{\downarrow}$, **b**) vertical velocities, and in the strength of the overturning circulation (I, **c**) predicted by coupled ocean-atmosphere models after an abrupt CO_2 quadrupling (solid circles, shown only when at least 10 model results are available). Also reported are estimates from the non-mitigated RCP8.5 climate change scenario around 2090 (open squares), and from $4xCO_2$ atmosphere-only experiments with fixed SSTs in realistic (stars) and aqua-planet (open circles) configurations. Vertical bars show ± one standard deviation of individual model results around the multi-model mean.
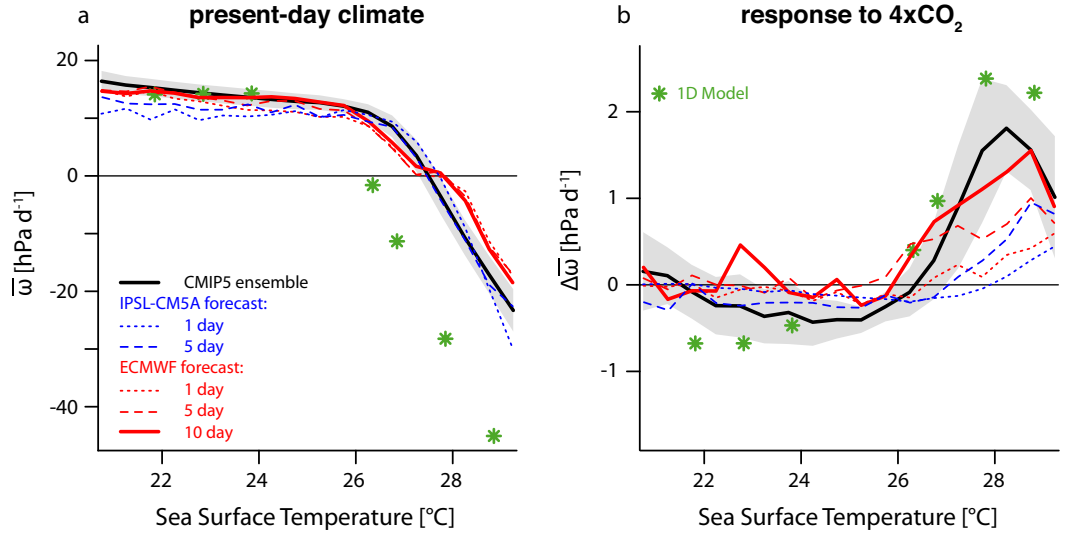
3

Figure 4: **Interpretation and time scale of the direct effect of CO_2 on large-scale vertical motions.** Monthly-mean $\bar{\omega}$ predicted by CMIP5 atmospheric GCMs over tropical oceans composited by sea-surface temperatures (SSTs) in the present-day climate (**a**), and its change when atmospheric CO_2 is quadruped but SSTs are kept unchanged ($4xCO_2$-$1xCO_2$, **b**). The black line shows multi-model mean values and the shaded area the inter-model standard deviation within each SST bin. Results from single-column (1D) simulations run in the "weak temperature gradient" approximation are shown by green stars. These simulations are compared with short atmospheric forecasts (at fixed forecast times) performed in $1xCO_2$ and $4xCO_2$ conditions using either a climate model (IPSL-CM5A) or an operational weather forecasting model (ECMWF).

4

Robust direct effect of carbon dioxide on tropical circulation and regional precipitation

Sandrine Bony[1,*], Gilles Bellon[2], Daniel Klocke[3], Steven Sherwood[4], Solange Fermepin[1] and Sébastien Denvil[1]

1: LMD/IPSL, CNRS, Université Pierre et Marie Curie, Paris, France

2: CNRM/GAME, CNRS, Météo-France, Toulouse, France

3: European Centre for Medium-Range Weather Forecasts, Reading, United Kingdom

4: Centre of Excellence for Climate System Science, University of New South Wales, Sydney, Australia

Supplementary Material

* Corresponding author address:

Sandrine Bony

LMD/IPSL, CNRS

UPMC, case courrier 99

4 Place Jussieu

75252 Paris cedex 05

France

Email: bony@lmd.jussieu.fr

Tel: 33-1-44 27 50 14

Fax: 33-1-44 27 62 72

CMIP5 inter-comparison project, models and experiments.

CMIP5 is an international model inter-comparison and analysis project coordinated by the Working Group on Coupled Models (WGCM) of the World Climate Research Programme (WCRP). An introduction to CMIP5 can be found in Meehl and Bony (2011), and CMIP5 experiments are summarised in Taylor et al. (2012). CMIP5 model outputs are available through the Earth System Grid Federation archive (Williams et al. 2011, $http://cmip-pcmdi.llnl.gov/cmip5$), and analysis results are assessed by the Fifth Assessment Report of the Intergovernmental Panel on Climate Change (IPCC AR5).

In CMIP5, an ensemble of climate models is used in a wide variety of experiments and in a spectrum of configurations of different complexities. It includes idealised experiments designed to better understand key aspects of climate change and to better interpret inter-model differences. For instance, the influence of the CO_2 radiative forcing on climate can be investigated :

- through coupled ocean-atmosphere experiments in which the CO_2 increases progressively with time (e.g. $+1\%$ CO_2/year experiment) or is abruptly quadrupled and then held fixed ('abrupt4xCO2' experiment);

- by comparing 1xCO2 and 4xCO2 atmosphere-only experiments where sea surface temperatures are kept fixed, using an SST distribution which is derived either from observations ('amip', 'amip4xCO_2') or from a climatology of the pre-industrial control run ('sstClim' and 'sstClim4xCO_2');

- by comparing 1xCO2 and 4xCO2 atmosphere-only experiments in a highly idealised configuration assuming that the Earth is covered by oceans only ('aquaControl', 'aqua4xCO2');

- in climate change scenarios, including one which assumes a socio-economic pathway where humans continue to use fossil fuels with no mitigation ('RCP8.5', Moss et al. 2010).

The different CMIP5 experiments are presented more extensively in Taylor et al. (2012). Table S1 presents the list of CMIP5 climate models and experiments analysed in this study. The number of available realisations of each experiment differs amongst models. To ensure that multi-model mean results are not biased towards models for which more realisations are available, for each model we use only one realisation of each experiment. As at the time of this study model outputs were unavailable or incomplete for some of the experiments, the number of models considered depends on the experiment under consideration. The water budget analysis and subsequent decomposition of precipitation changes into dynamic and thermodynamic components are performed at the monthly time scale for each experiment and each model on native model grids (in the IPSL-CM5A-LR GCM, the sum of the monthly-mean components diagnosed offline differed by less than 5% from the monthly-mean

2

precipitation actually predicted by the model at each timestep, suggesting that non-linearities are not a significant limitation of the analysis). Then, model results are interpolated onto a common 2.5^o x 2.5^o horizontal grid, and multi-model averages are computed. Individual model results are shown in this Supplementary Material. The results from 'amip4xCO$_2$' and 'sstClim4xCO$_2$' experiments being fairly similar (Table 2), their average is reported in Figure 3.

Evolution of tropical precipitation with CO$_2$ and surface warming.

Figure S1 summarises the evolution of the annual-mean tropical precipitation under increased CO$_2$ and surface warming over land and ocean regions, in regimes of large-scale ascent (also named convective regimes) and in regimes of large-scale subsidence. Here, large-scale circulation regimes are defined from the pre-industrial climate (piControl), and are thus affected by both thermodynamic and dynamic changes.

Over ocean, precipitation increases with surface warming in both regimes. In convective regimes, dynamic changes tend to reduce precipitation (owing to the direct effect of CO$_2$ and to the weakening of large-scale vertical motions with surface warming) while the thermodynamic component increases precipitation (Figure S2). The opposite occurs in subsidence regimes. Over land, the dynamic and thermodynamic components have antagonist influences on precipitation.

Both over land and ocean, systematic changes of precipitation from direct CO$_2$ forcing are of comparable magnitude to those from surface warming.

Interpretation of the thermodynamic component (ΔP_{ther}) of tropical precipitation changes.

Figure S2 presents an analysis of the present-day tropical precipitation in atmospheric circulation regimes defined from $\bar{\omega}$, and of the sensitivity of tropical precipitation to sea surface temperature changes in abrupt 4xCO2 coupled ocean-atmosphere experiments (relative to the pre-industrial climate). Using the methodology presented in Methods, the mean precipitation and the precipitation change are first decomposed into different components associated with the different terms of the vertically-integrated water budget. Then, time series of each component are stratified by monthly-mean $\bar{\omega}$ values using bins of 5 hPa/day. Finally, the sensitivity to temperature is estimated within each dynamical regime as the linear regression coefficient of precipitation changes (or its components) against sea surface temperature changes. The probability distribution function of $\bar{\omega}$ (Bony et al. 2004) is shown at the bottom of each figure panel.

This figure shows the prominent contributions of surface evaporation (E) and of the vertical advection term ($\bar{\omega}\Gamma_q$) to the regional water budget and precipitation. It also shows that in convective regimes ($\bar{\omega}<0$), the sign and the magnitude of precipitation changes with surface temperature are pri-

marily explained by two components: the Clausius-Clapeyron thermodynamic relationship (which predicts an increase of the water holding capacity of the atmosphere with temperature of about 7.5 %/K), and the increase of surface evaporation (about 2 %/K, Held and Soden 2006). In subsidence regimes ($\bar{\omega}>0$), the precipitation change with temperature results from two main (antagonist) contributions: the increase of water vapour with temperature associated with the Clausius-Clapeyron relationship (which makes the vertical advection term more negative in a warmer climate), and the increase of surface evaporation (by more than 2 %/K).

Thermodynamic component of regional precipitation changes simulated by individual CMIP5 models.

Figures 1 and 2 show multi-model regional patterns of the thermodynamic component of precipitation changes. As discussed in the main text and explained by Figure S2, the sign and magnitude of this component are closely related to the large-scale dynamical regime under consideration ($\bar{\omega}$) and to the Clausius-Clapeyron relationship. For this reason, one expects the geographical distribution of this component to be also closely related to the climatological distribution of dynamical regimes in the unperturbed (e.g. pre-industrial) climate. This is verified by Figure S3 which compares, for each CMIP5 model, the climatological distribution of precipitation in the pre-industrial climate with the normalised thermodynamic component ($\Delta P_{\text{ther}}/\Delta T_s$) inferred from abrupt4xCO2 experiments. Spatial correlation coefficients between the patterns of precipitation climatology in the pre-industrial climate and the thermodynamic component of precipitation change in the RCP8.5 scenario range from 0.39 (FGOALS-s2 model) to 0.84 (IPSL-CM5A-LR model), and equal 0.70 (with a standard deviation of 0.12) on average over the models.

The strong correlation between the two patterns is further demonstrated by Figure S4 which shows the multi-model mean annual precipitation climatology, the multi-model mean normalised thermodynamic component and the correlation among the climatology and the thermodynamic component computed across CMIP5 models.

Direct effect of CO_2 on large-scale atmospheric vertical motions and precipitation in the individual CMIP5 models.

Table S2 presents the fractional change in $\bar{\omega}^{\uparrow}$ and $\bar{\omega}^{\downarrow}$ predicted by individual CMIP5 models in 4xCO2 atmosphere-only experiments forced by a climatology of pre-industrial sea surface temperatures (sstClim). We also report multi-model means for these experiments and for another CMIP5 atmosphere-only experiment (referred to as amip) where sea-surface temperatures are prescribed from present-day observations instead of pre-industrial climatologies from model results. Although the sign of circulation changes is robust across models, we note inter-model differences in the magni-

4

tude of $\bar{\omega}^{\uparrow}$ and $\bar{\omega}^{\downarrow}$ changes, especially over land in convective areas. The inter-model spread in the continental fast response might result in part from the fast response to transient land-sea contrasts.

Maps of the fast dynamic component of precipitation changes (ΔP_{dyn}) for each CMIP5 model (left panels of Figure S5) shows that each model predicts fast and substantial changes in large-scale vertical motion shortly after the CO_2 increase, even when surface warming is still small (less or about 1 K over the first year). The response is qualitatively consistent amongst models at first order (tendency to predict more precipitation and stronger large-scale rising motions in convective land regions, tendency to predict less precipitation over convective areas of tropical oceans). However, Figure S5 also reveals inter-model differences in the simulated patterns, likely due in part to inter-model differences in the simulated circulation patterns of the pre-industrial climate.

Figure S5 also shows that the fast dynamic component of precipitation changes (left panels) inferred from idealised abrupt4xCO2 experiments is of similar order of magnitude and exhibits many similarities over tropical oceans with the long-term pattern of the dynamic component (right panels) inferred from RCP8.5 climate change experiments at the end of the 21st century.

Using the IPSL-CM5A-LR model, we verified that using one or several realisations of the abrupt4xCO2 coupled ocean-atmosphere simulation does not qualitatively change the results.

The correlation between the fast and long-term dynamical patterns is confirmed by the correlation map shown in Figure S6. Over land areas (e.g. over Africa), the signs of the fast and long-term dynamic components are often opposite. This is consistent with the antagonist effects of CO_2 and temperature (local surface warming and transient land-sea contrasts) on large-scale rising motions over land (Figure 3). Over many areas of tropical oceans, but also over part of Amazonia and of the Sahel, the fast ΔP_{dyn} correlates quite strongly with the long-term component (correlation across models > 0.6 or 0.8). Gaining confidence in the pattern of the fast dynamic component may thus be a way to gain confidence in a key component of long-term precipitation projections.

Response of the tropical precipitation to increased CO_2 predicted by the ECMWF-IFS model.

Figure S7 shows the monthly-mean tropical precipitation for October 2011, and its response to a quadrupling of CO_2, predicted by the ECMWF-IFS model for different forecast times (after 1 day, 5 days and 10 days). Note the reduction over ocean of large-scale rising motion and precipitation in regions of present-day convection and high-rain. Changes in precipitation are much weaker in regions of present-day subsidence and suppressed precipitation, suggesting a slower response of large-scale vertical motions to increased CO_2 in subsidence regions than in convective regions. Precipitation increases over land owing to the increase of convective instability (associated with a larger warming near the surface than aloft).

References

- Bony, S., Dufresne, J.-L., Le Treut, H., Morcrette, J.-J. & Senior, C. On dynamic and thermodynamic components of cloud changes. *Clim. Dyn.* **22**, 71-86 (2004).

- Meehl, G. A. & Bony, S. Introduction to CMIP5. *CLIVAR Exchanges* **56**, Vol.16, No.2, 4-5 (2011).

- Moss, R. et al. A new approach to scenario development for the IPCC Fifth Assessment Report. *Nature*, **463**, doi:10.1038/nature08823 (2010).

- Taylor, K. E., Stouffer, R. J. & Meehl, G. A. An Overview of CMIP5 and the experiment design. *Bull. Amer. Meteor. Soc.*, **93**, 485-498, doi:10.1175/BAMS-D-11-00094.1 (2012).

- Williams, D. N. et al. The Earth System Grid Federation: software framework supporting CMIP5 data analysis and dissemination. *CLIVAR Exchanges* **56**, Vol.16, No.2, 4-5 (2011).

Modeling Center	Model version	Coupled ocean-atmosphere experiments			Atmosphere-only experiments		Aqua-planet experiments
		pre-industrial	abrupt 4xCO2	RCP8.5 scenario	sstClim & sstClim4xCO2	amip & amip4xCO2	aquaControl & aqua4xCO2
BCC, China	bcc-csm1-1	X	X	X			
CCCma, Canada	CanESM2	X	X	X	X	X	
CNRM/CERFACS, France	CNRM-CM5	X	X	X		X	X
LASG-CESS, China	FGOALS-g2	X	X	X		X	X
LASG-IAP, China	FGOALS-s2	X	X	X	X		X
MOHC, UK	HadGEM2-ES	X	X	X	X	X	X
INM, Russia	inmcm4	X	X		X		
IPSL, France	IPSL-CM5A-LR	X	X	X	X	X	X
IPSL, France	IPSL-CM5A-MR	X	X	X			
IPSL, France	IPSL-CM5B-LR	X	X	X			X
MIROC, Japan	MIROC5	X	X	X	X	X	X
MIROC, Japan	MIROC-ESM	X	X	X			
MPI-M, Germany	MPI-ESM-LR	X	X	X	X	X	X
MPI-M, Germany	MPI-ESM-P	X	X				
MRI, Japan	MRI-CGCM3	X	X	X	X		
NCC, Norway	NorESM1-M	X	X	X	X		

Table S1: List of CMIP5 climate models and experiments analysed in this study (X indicates that a realisation of the experiment was used; the absence of X indicates that model outputs were unavailable or incomplete at the time of the analysis). See Methods or Taylor et al. (2012) for a presentation of the different CMIP5 experiments.

	Ocean		Land	
CMIP5	$\Delta\bar{\omega}^{\uparrow}/\bar{\omega}^{\uparrow}$	$\Delta\bar{\omega}^{\downarrow}/\bar{\omega}^{\downarrow}$	$\Delta\bar{\omega}^{\uparrow}/\bar{\omega}^{\uparrow}$	$\Delta\bar{\omega}^{\downarrow}/\bar{\omega}^{\downarrow}$
Models	[%]	[%]	[%]	[%]
CanESM2	-3.56	-2.56	8.85	-0.73
FGOALS-s2	-5.07	-2.71	3.98	-1.55
HadGEM2-ES	-5.07	-3.05	9.73	-0.91
inmcm4	-1.49	-2.09	1.91	-0.91
IPSL-CM5A-LR	-4.28	-2.28	0.71	-2.39
MIROC5	-4.57	-1.92	5.26	-0.65
MPI-ESM-LR	-2.59	-1.38	8.24	-1.83
MRI-CGCM3	-5.21	-3.26	2.09	-1.21
NorESM1-M	-3.18	-1.17	10.06	-0.78
MMM sstClim4xCO2	-3.89 ± 1.29	-2.27 ± 0.71	5.65 ± 3.66	-1.22 ± 0.59
MMM amip4xCO2	-3.72 ± 1.19	-2.49 ± 0.84	3.91 ± 1.88	-0.65 ± 1.16

Table S2: For tropical ocean and land regions : 30-year averages of the fractional change between 4xCO2 and 1xCO2 conditions of $\bar{\omega}^{\uparrow}$ and $\bar{\omega}^{\downarrow}$ predicted by CMIP5 models in atmosphere-only experiments using prescribed sea surface temperatures from pre-industrial control simulations and unchanged between 1xCO2 and 4xCO2 experiments (the table reports sstClim4xCO2-sstClim differences). Multi-model mean (MMM) results are reported both for sstClim4xCO2-sstClim experiments and for amip4xCO2-amip experiments (in amip experiments, SSTs are prescribed from observations). For comparison, model standard deviations in 1xCO2 climate (expressed as a percentage of climatological means) associated with natural variability are 1.89 ± 0.84 % and 1.08 ± 0.48 % over ocean for $\bar{\omega}^{\uparrow}$ and $\bar{\omega}^{\downarrow}$, respectively, and 1.34 ± 0.36 % and 1.96 ± 0.69 % over land.
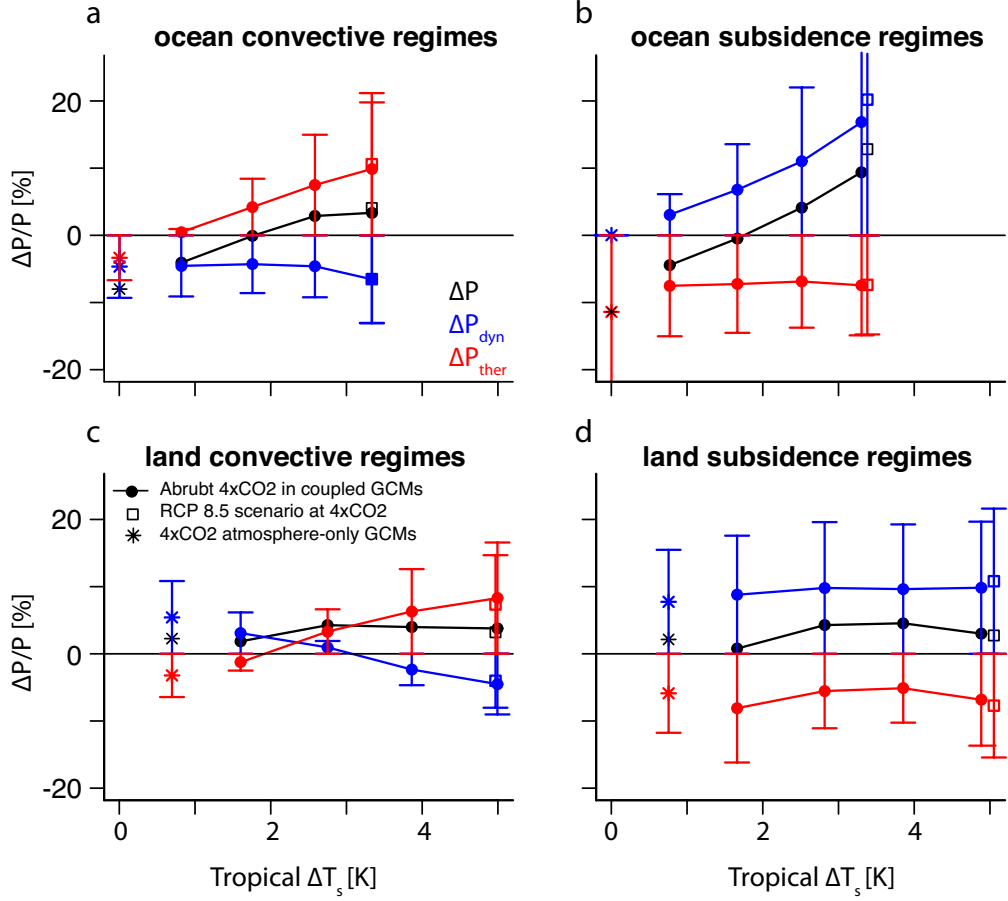
Figure S1: **Evolution of precipitation as a function of CO_2 and surface warming.** The different panels show the evolution, as a function of tropical surface warming, of the annual-mean precipitation ($\Delta P = \Delta P_{\mathrm{dyn}} + \Delta P_{\mathrm{ther}}$) predicted by CMIP5 models in pre-industrial regimes of large-scale ascent ($\bar{\omega} < 0$, also named "convective" regimes, left panels) or large-scale subsidence ($\bar{\omega} > 0$, right panels). Results are reported for several CMIP5 experiments : for abrupt4xCO2 coupled ocean-atmosphere experiments (first 30 years of simulation after CO_2 quadrupling), for non-mitigated climate change scenario experiments at the end of the century (RCP8.5, around 2090), and for equilibrium atmosphere-only experiments in which the CO_2 concentration is quadrupled but sea surface temperature are kept unchanged (sstClim4xCO2, averaged over 30-years). Fractional changes relative to pre-industrial values are expressed in %. Vertical bars show $\pm$ one inter-model standard deviation of individual model results around the multi-model mean.
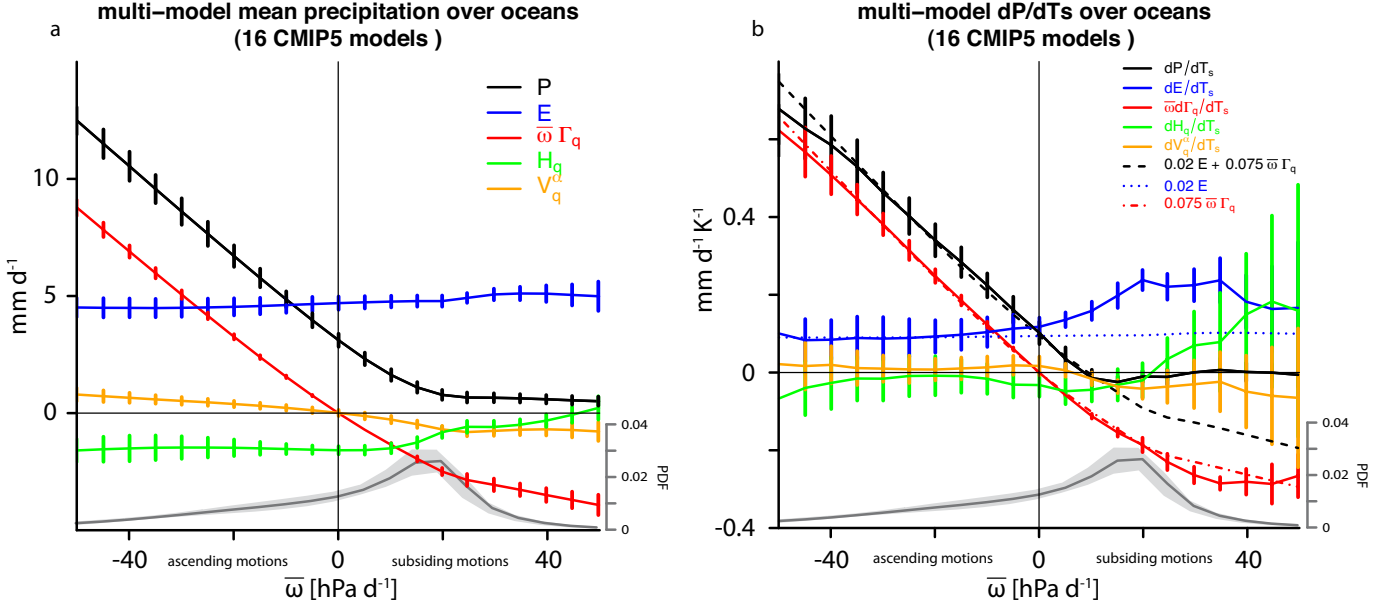
Figure S2: **Tropical precipitation analysis in large-scale circulation regimes. (a)** Monthly-mean precipitation (P) and its different components ($P = E + \bar{\omega}\Gamma_q + H_q + V_q^\alpha$, see the Methods section for the definition of each term) composited as a function of $\bar{\omega}$ in the pre-industrial climate (the compositing methodology is explained in Bony et al. 2004). **(b)** Sensitivity of precipitation, and of its different components, to sea surface temperature changes estimated through linear regression from abrupt4xCO2 simulations. Also reported in **b** are approximate sensitivities of the vertical advection term predicted by the Clausius-Clapeyron relationship (7.5 % K^{-1}), surface evaporation (2 % K^{-1}) and their sum. Each panel shows multi-model averages (thick lines) and $\pm$ one standard deviation (vertical bars) of individual model results. At the bottom of each panel, the multi-model mean probability distribution function of $\bar{\omega}$ in pre-industrial conditions (the shaded area shows the inter-model standard deviation) shows the statistical weight of the different circulation regimes over tropical oceans.
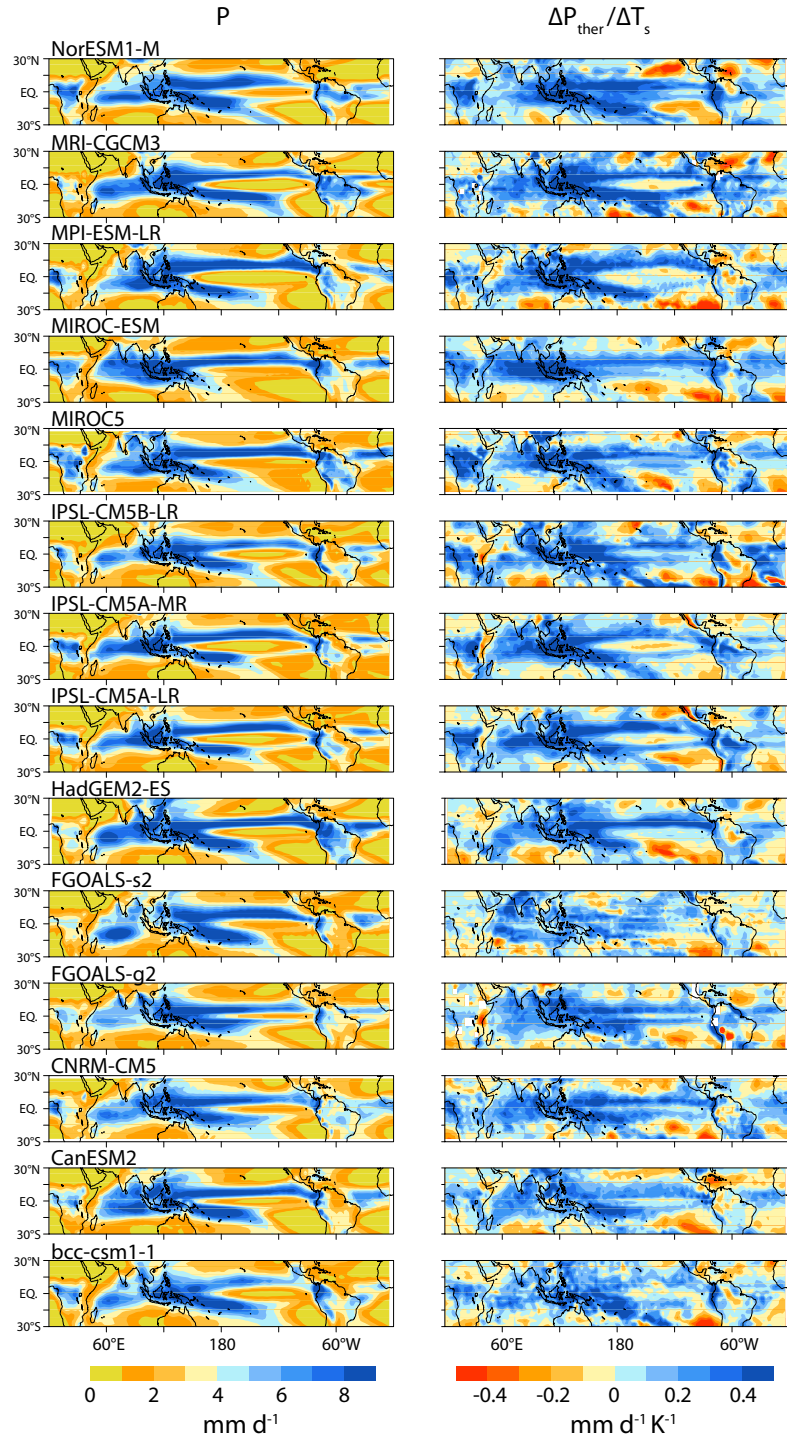
Figure S3: **Precipitation climatology and thermodynamic component of precipitation changes predicted by individual CMIP5 OAGCMs.** Left panels show climatological distributions of precipitation predicted by CMIP5 coupled ocean-atmosphere models in pre-industrial climate (30-year average from piControl experiment), and right panels show the regional patterns of the thermodynamic component of precipitation changes normalised by surface warming ($\Delta P_{\text{ther}}/\Delta T_s$, expressed in $\text{mm}\,\text{d}^{-1}\,\text{K}^{-1}$) inferred from abrupt4xCO2 experiments as climate is warming.
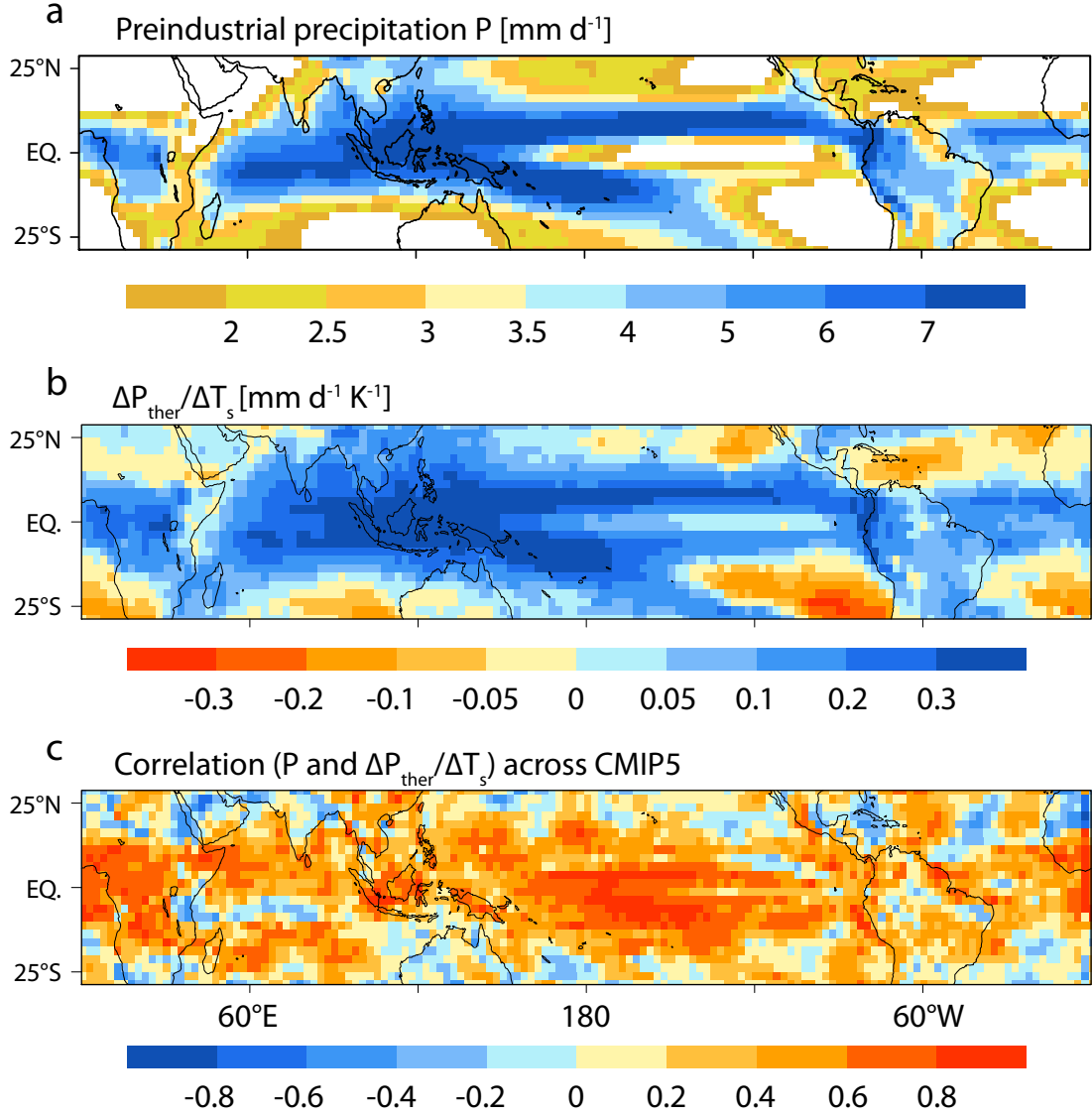
Figure S4: **Correlation between precipitation climatology and the thermodynamic component of precipitation changes (a)** Multi-model mean pattern of annual precipitation (in $\mathrm{mm\,d^{-1}}$) derived from 16 CMIP5 OAGCMs in the pre-industrial climate (piControl). **(b)** Multi-model mean pattern of the thermodynamic component of precipitation changes normalised by the local surface warming ($\Delta P_{\mathrm{ther}}/\Delta T_s$, expressed in $\mathrm{mm\,d^{-1}\,K^{-1}}$) inferred from the same models in abrupt4xCO2 experiments. **(c)** Correlation (computed across 16 CMIP5 models) between the precipitation climatology and the thermodynamic component predicted by individual models.
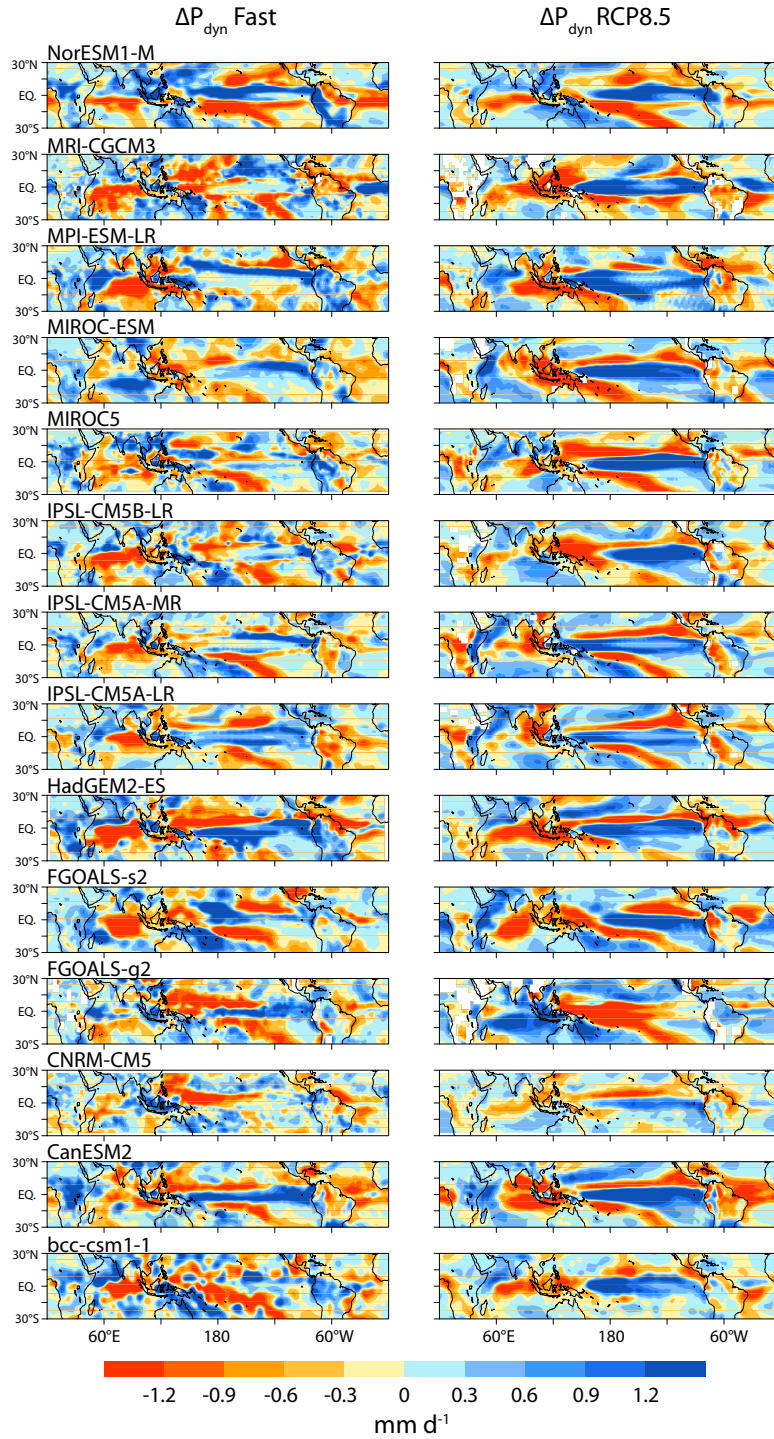
12

Figure S5: **Fast and long-term dynamic components of precipitation changes predicted by individual CMIP5 OAGCMs.** Left panels show the fast dynamic component of precipitation changes (ΔP_{dyn}, in mm d^{-1}) inferred from abrupt4xCO2 experiments during the first year after CO$_2$ quadrupling. Right panels show the dynamic component of precipitation changes predicted by the same models in a non-mitigated climate change scenario (RCP8.5) at the end of the century (around 2090).
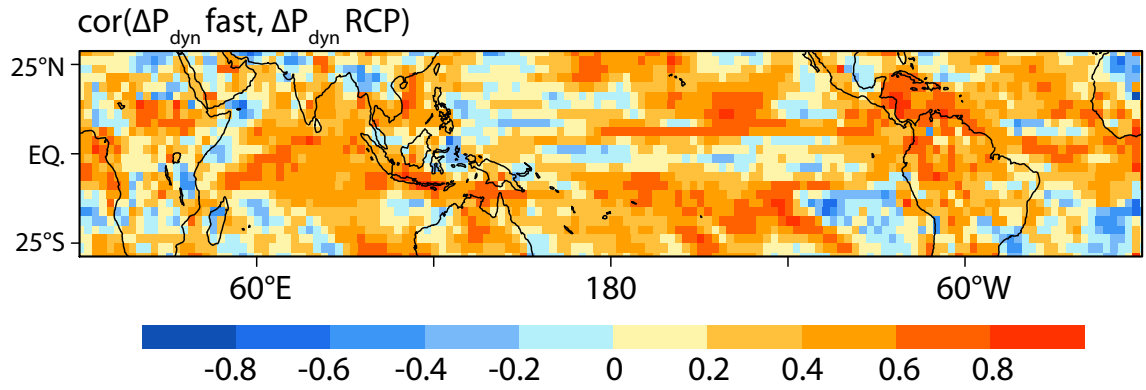
13

Figure S6: **Inter-model correlation between fast and long-term dynamic components of precipitation changes.** The figure shows the linear correlation coefficient (computed across 14 CMIP5 models) between the fast dynamic response of precipitation to increased CO_2 (ΔP_{dyn} fast, inferred from the first year of abrupt4xCO2 experiments) and the long-term dynamic response of precipitation (ΔP_{dyn} RCP, estimated from RCP8.5 experiments at the end of the 21st century).
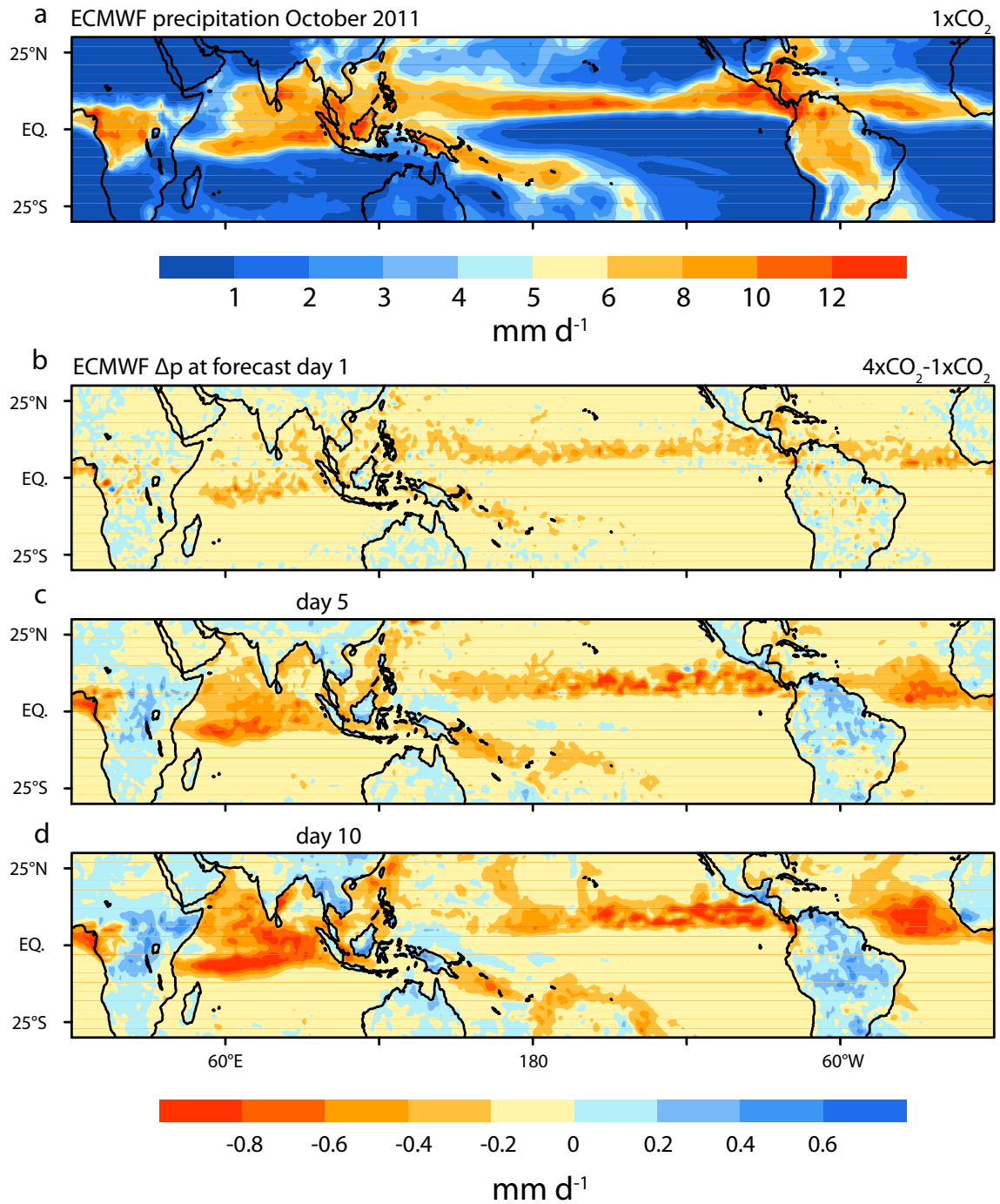
Figure S7: **Direct effect of CO_2 simulated by an operational Numerical Weather Prediction model.** **(a)** Monthly-mean tropical precipitation derived from ECMWF-IFS forecasts for October 2011 using present-day CO_2 concentration. **(b-d)** Change in the October 2011 monthly-mean precipitation associated with a quadrupling of the CO_2 concentration in the atmosphere, shown for different forecast times (1 day, 5 days and 10 days).
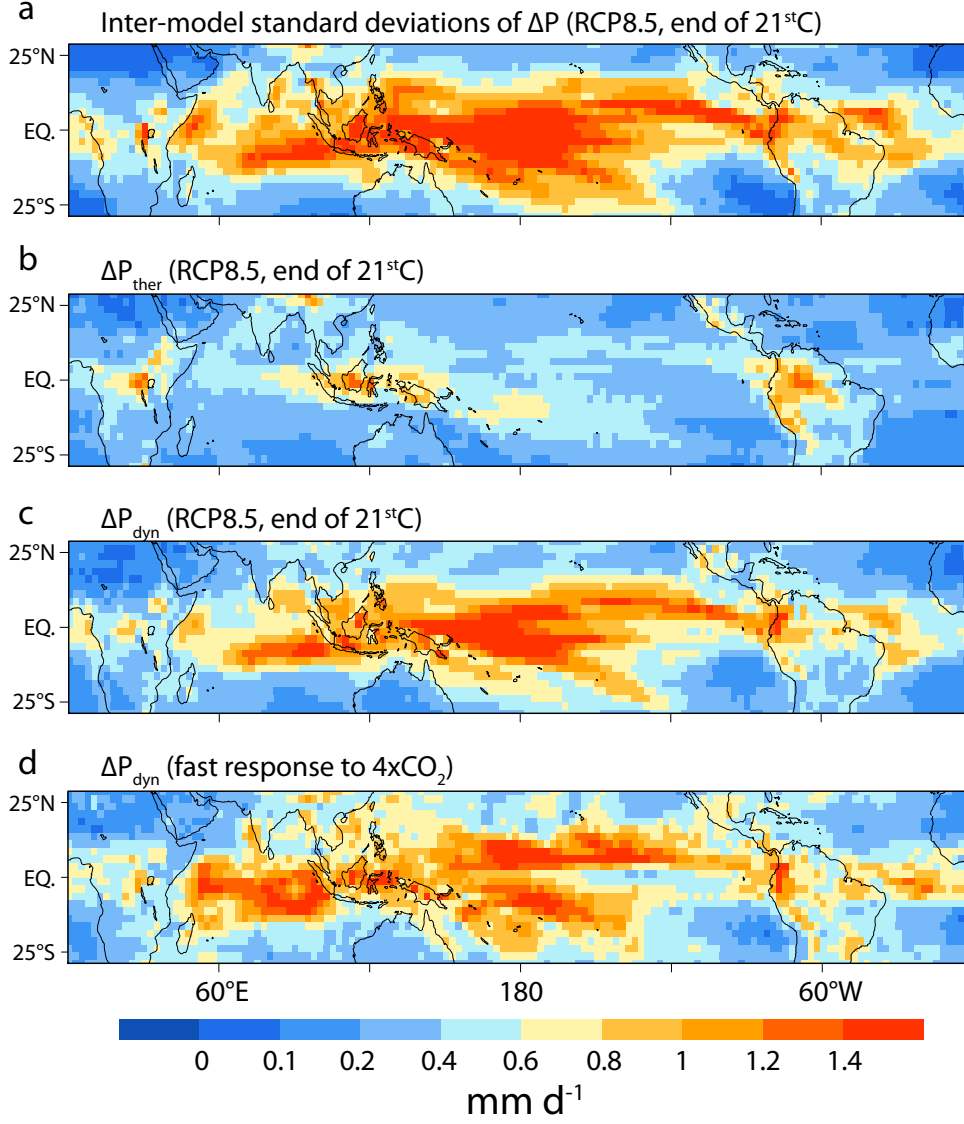
Figure S8: **Inter-model spread of regional precipitation projections in the tropics. (a)** Spread (inter-model standard deviation, in $mm\,d^{-1}$) of precipitation changes projected by 14 CMIP5 OAGCMs in the RCP8.5 scenario at the end of the 21st century. **(b) and (c)** Spread of the thermodynamic and dynamic components of precipitation changes in the same models and the same scenario. **(d)** Spread of the fast dynamic component of precipitation changes inferred from the first simulated year of abrupt4xCO2 experiments. The tropical-mean standard deviations of the different panels from top to bottom are: 0.69, 0.35, 0.58 and 0.63 $mm\,d^{-1}$.

16